Tissue engineering of retina through high resolution 3-dimensional inkjet bioprinting

Elahe Masaeli, Valérie Forster, Serge Picaud, Fereshte Karamali, Mohammad Hossein Nasr-Esfahani, Christophe Marquette

Biofabrication

International Society for Biofabrication

ACCEPTED MANUSCRIPT

Tissue engineering of retina through high resolution 3-dimentional inkjet bioprinting

To cite this article before publication: Elahe Masaeli *et al* 2019 *Biofabrication* in press https://doi.org/10.1088/1758-5090/ab4a20

Tissue Engineering of Retina through High Resolution 3-dimentional Inkjet Bioprinting

Elahe Masaeli [1, 2], Valérie Forster [3], Serge Picaud [3], Fereshte Karamali [1], Mohammad Hossein Nasr-Esfahani [1], Christophe Marquette [2]

[1] Department of Cellular Biotechnology, Cell Science Research Center, Royan Institute for Biotechnology, ACECR, Isfahan, Iran.

[2] 3d.FAB, Univ Lyon, Université Lyon1, CNRS, INSA, CPE-Lyon, ICBMS, UMR 5246, Bat. Lederer, 1 rue Victor Grignard, 69100 Villeurbanne, France.

[3] Institut de la Vision, 17 rue Moreau, 75012 Paris.

KEYWORDS: Retina Pigmented Epithelium; Photoreceptors; Bioprinting; Tissue Engineering

ABSTRACT: The mammalian retina contains multiple cellular layers, each carrying out a specific task. Such a controlled organization should (Yue *et al.*, 2015)be considered as a crucial factor for designing retinal therapies. The maintenance of retinal layered complexity through the use of scaffold-free techniques has recently emerged as a promising approach for clinical ocular tissue engineering.

In an attempt to fabricate such layered retinal model, we are proposing herein a unique inkjet bioprinting system applied to the deposition of a photoreceptor cell (PRs) layer on top of a bioprinted retinal pigment epithelium (RPE), in a precise arrangement and without any carrier material. The results showed that, after bioprinting, both RPE and PRs were well positioned in a layered structure and expressed their structural markers, which was further demonstrated by ZO1, MITF, rhodopsin, opsin B, opsin R/G and PNA immunostaining, 3 days after bioprinting. We also showed that considerable amounts of human vascular endothelial growth factor (hVEGF) were released from the RPE printed layer, which confirmed formation of a functional RPE monolayer after bioprinting. Microstructures of bioprinted cells as well as phagocytosis of photoreceptor outer segments by apical RPE microvilli was finally established through transmission electron microscopy (TEM) imaging. In summary, using this carrier-free bioprinting method, it was possible to develop a reasonable *in vitro* retina model for studding some sight-threatening diseases such as age-related macular degeneration (AMD) and retinitis pigmentosa (RP).

INTRODUCTION

The retina is a complex photosensitive layer of the central nervous system, which covers inner surface of eye cup and is vital for maintenance of vision (Singh *et al.*, 2018). Vertebrate retina contains different parallel cellular layers, including inner neuroepithelial and outer pigmented epithelial layers. Among neural cells, light-sensing photoreceptors, i.e. cones and rods, are responsible of visual phototransduction in eye. To begin the process of seeing, light enters the eye, traverse most of inner layers, and finally impinges on the outer segments of photoreceptors. Photoreceptors then transduce photon energy into electric signals that are conveyed to other retinal neurons. The retinal pigment epithelium (RPE) consists of a cell monolayer situated between the photoreceptors and the choroid. This epithelium supports and insulates the photoreceptors to increase visual resolution at high light levels.

Since these photoreceptors are fully differentiated neurons lacking regenerative capacity (Tropepe *et al.*, 2000), dysfunction of these retinal layers leads to several irreversible sight-threatening diseases such as age-related macular degeneration (AMD) and retinitis pigmentosa (RP). These diseases are then particularly attractive challenges for regenerative medicine developments (Ramsden *et al.*, 2013; Trese *et al.*, 2012).

In these diseases, areas of RPE atrophy are associated with photoreceptor degeneration. Hence, most of stem cell-based therapies focus on replacing RPE to maintain normal function of photoreceptors or attempt to restore their integrity in the affected eye (Trese *et al.*, 2012). Unfortunately, several challenges such as selection of cell delivery method, limited integration of grafted cells and incomplete differentiation to a specific fate hinder the success of function regeneration (Yao *et al.*, 2011).

Accordingly, in recent studies, tissue engineering based strategies have been widely applied as an alternative approach to address aforementioned problems. Synthetic and natural polymeric scaffolds with well-defined requirements, such as biocompatibility in the sub-retinal space, ultra-fine structure, and appropriate physico-mechanical properties for implantation, has been introduced to guide retinal repair (Yao *et al.*, 2011; Trese *et al.*, 2012; Tomita *et al.*, 2005). Nevertheless, inflammatory side effects and loose integration of RPE layer to the underlying choroid, that sustains the RPE and photoreceptors' function, are two main challenges in applying biodegradable scaffolds for retinal regeneration.

Cell sheet engineering is another alternative, which does not rely on a polymer scaffold. Such a strategy is based on harvesting cultured cells as intact sheets along with their extracellular matrix (ECM), and combine them to form tissue-like structures (Mokhtarinia *et al.*, 2018). In previous studies, cellular monolayers from different cell sources have been generated using conventional scaffold-free engineering approaches to treat retinal degenerative diseases (Yaji *et al.*, 2009; Yang *et al.*, 2006; Umemoto *et al.*, 2013). However, retinal cellular complexity, as a crucial requirement for effective function of engineered grafts, has not been addressed in these studies.

Additive manufacturing for direct patterning and depositing of living materials, known as 3D bioprinting, has been increasingly used to fabricate cell based 3D structures (De Maria *et al.*, 2017). Indeed, the capability of 3D bioprinter systems (laser-based, inkjet-based or extrusion-based) for layer-by-layer precise positioning of bio-components in cell-friendly conditions bring various advantages over exiting fabrication technologies, the principal one being the capability to generate complex and predefined 3D geometries (Tasoglu and Demirci, 2013). The structures obtained through 3D bioprinting were then shown to be useful for the development of 3D constructs with tailored biological heterogeneity, directly apply in tissue engineering and

regenerative medicine studies (Kolesky *et al.*, 2014; Xu *et al.*, 2013; Pourchet *et al.*, 2017), but also cell-based sensors (Dias *et al.*, 2014), drug screening (Jorge *et al.*, 2012) and tumor models production (Yu *et al.*, 2014). The definition of these geometries is directly related to the bioprinting technique used, for example, the highest precision (single cell deposition) reached using laser-based systems (Guillotin and Guillemot, 2011; da Silva *et al.*), high resolution (tenth of cells or nL drop) using inkjet-based technique and medium resolution but large volume geometries using extrusion-based bioprinters. The herein reported study aimed at demonstrating the capability of inkjet-based bioprinting to recapitulate retinal components. Indeed, layer-by-layer bioprinting process matches nicely with the native multilayered anatomy of the retina and cells precise deposition through inkjet bioprinting might help control their subsequent interactions.

To the best of our knowledge, there have been very few reports on attempt to construct multilayered tissue-engineered retinal tissue through bioprinting. Two studies in the field of successive bioprinting of retinoblastoma cells on RPE layer are among the seldom efforts made in this area (Shi *et al.*, 2017; Shi *et al.*, 2018).

The objective of the present study was then to develop a three-dimensional retina model, which may have clinical implications for retinal regeneration therapies. In order to fabricate this construct, inkjet-based bioprinting strategy was applied to deposit matured and differentiated photoreceptors on RPE layer in a predefined arrangement to create complex double-cell sheets. A thin layer of gelatin methacrylate (GelMa) was also explored to mimic Bruch's membrane before RPE deposition.

MATERIALS & METHODS

Gelatin Methacrylate (GelMa) Solution Preparation and Coating

To simulate the basement membrane of RPE (i.e. Bruch's membrane), GelMa coating was applied to circular glass coverslips (0.5 mm thick, 17 mm diameter, T&Q, China), subsequently used as substrate for bioprinting. Coating solution was prepared by dissolving 2 mg of GelMa (Sigma 900496, France) in 10 mL of a 1.5 % (w/v) solution of Irgacure 2959 (Sigma 410896, France) in dimethyl sulfoxide (Merck 102952, Germany) for 30 minutes at 55 °C. Once dissolved, the solution was centrifuged to remove air bubbles. Stock GelMa solution was stored in a light tight container at 2-8 °C to prevent unintentional crosslinking by ambient light. Prior GelMa thin layer spin coating, the circular glass coverslips were degreased with acetone, rinsed with deionized water and air dried. 200 µl GelMa stock solution was then dropped onto each cover glass coverslips rotating at 3000 rpm and coated for 30 seconds using a WS-650MZ spin coater (Laurell, USA). After spin coating, GelMa polymerization was performed by placing the coated coverslips in a UV chamber (BLX-E254, Bio-Link, Fisher Biotec, Australia) for 30 minutes.

RPE Cell Culture and Labeling

RPE cell line ARPE-19 (ATCC CRL-2302, France) was cultured in DMEM-F12 medium (ATCC 30-2006, France) supplemented with 10% fetal bovine serum (FBS, Gibco 10270, France) and 1% penicillin/streptomycin (Gibco 15140, France). Before inkjet bioprinting, RPE cells were stained with fluorescent dye (PKH67 GL, Sigma, France) according to the manufacturer's instructions. Briefly, 1×10^7 cells were suspended in 1 ml 2×10^{-6}M PKH 67 solution in diluent C (provided in the staining kit), and incubated for 1-5 minutes at room temperature with periodic mixing. The excess staining reagents were first diluted with an equal volume of culture medium supplemented

with 10% FBS, then discarded through centrifugation for 10 minutes at 800 rpm. The cellular pellet was recovered and washed again with supplemented culture medium.

Isolation of Photoreceptors (PRs)

Adult pig ocular globes were obtained from the surgical school of University Lyon 1 immediately after euthanasia and transported to the laboratory in ice-cold CO_2-independent Dulbecco's modified Eagle's medium (DMEM) (Gibco 18045, France) supplemented with 10 mg/ml gentamicin (Gibco 15710, France). Dissection of the retina from ocular globes was performed in our laboratory, as described previously (Luo *et al.*, 2001).

Briefly, after immersion of the whole globe in two successive disinfection baths (PhagoSpray, Phagogene, France) and one CO_2-independent medium, the cornea with lens and vitreous attached was removed. Retina layer was separated from the posterior eye cup, cut into small pieces (1-2 mm) and subsequently washed twice with warm glucose solution in phosphate buffer saline (PBS, Gibco 14190, France) (1 g/L). Afterward, retina pieces were incubated in 4 Unit activated papain solution (Worthington LSO 3124, USA) at 37°C for 20 minutes and shaken gently every 10 minutes. To stop digestion step, 1 ml of Neurobasal-A medium (Nb-A, Invitrogen 10888, France) supplemented with 10% FBS and DNase I was applied. The tissue fragments were dissociated by gentle shaking of the tube for 10 seconds, after which the suspension was allowed to settle for 2 minutes. The supernatant containing PRs was carefully harvested, fresh Nb-A was added and the gentle shaking repeated. The suspension was allowed to settle for another 2 minutes, after which the supernatant was collected and pooled with the first one. The pellet was discarded, and the pooled supernatants were centrifuged for 5 minutes at 800 rpm and finally re-suspended in Nb-A supplemented with 2% B27 (Invitrogen 17504, France). Viable cell number was estimated after trypan blue vital dye exclusion. Schematic of PRs isolation has been illustrated in **Figure 2-A**.

Cells' Bioprinting

Micro-patterning of RPE and PRs arrays was performed using a piezoelectric inkjet dispenser S3 sciFLEXARRAYER (Scienion AG, Germany) used here as a non-contact bioprinter. The instrument has a three axis micro-positioning system (accuracy 10 µm) and is equipped with an 80 µm diameter glass nozzle. The vertical separation between the nozzle and the substrate was typically 500 µm. A stroboscopic camera allows visual monitoring to adjust piezo voltages and pulse durations for reliable droplet ejection. Single drop ejected from the nozzle has a mean volume of 300 pL under our experimental conditions. For RPE bioprinting, arrays of 50 deposition locations of 52 drops were dispensed within an array of 10×10 spots (spot pitch of 800 µm). For PRs bioprinting, arrays of 100 deposition locations of 52 drops were dispensed within an array of 10×10 spots (spot pitch of 800 µm) ***(Supplementary information 1***). Bioprinted constructs were cultivated in the culture medium of PRs containing Nb-A supplemented with 2% B27.

Cellular viability assay

Cell population growth assessments were performed using an *in vitro* viability assay kit (Sigma TOX8, France) based on resazurin enzymatic reduction by cell metabolic activity. Briefly, for each proliferation assay, cell culture supernatant was harvested and 10% (v/v) of resazurin dye was added to the culture medium. According to manufacturer's protocol, RPE cells with high density and enough metabolic activity were incubated just for 2 hours at 37°C, and subsequently assessed spectrophotometrically by monitoring the decrease in absorbance at a wavelength of 600 nm. Measures of the absorbance of 96-well plates were also performed at a reference wavelength of 690 nm and subtracted from the 600 nm measurements. Results of these cell population growth assays were then given as "Neat Absorbance" corresponding to OD_{600}-OD_{690}.

Actin Cytoskeleton Staining

Specific staining of cellular actin cytoskeleton was performed on bioprinted samples using 2 steps protocol. First, cellular constructs were fixed with 3.7% (v/v) paraformaldehyde (Sigma P6148, France) diluted in PBS for 30 minutes at room temperature and then washed 3 times with PBS. Afterward, the fixed constructs were permeabilized by Triton X-100 (Sigma T8787, France) at a concentration of 0.1% (v/v) in PBS for 10 minutes at room temperature, before incubation with 1:40 dilution in PBS of a solution of Alexafluor 546-labelled phalloidin (Molecular Probes A22283, France) for 40 minutes at room temperature. The constructs were counterstained with DAPI (Invitrogen D1306, France) at a concentration of 300 nM in PBS for 10 minutes at room temperature and investigated by confocal imaging.

Immunofluorescent labelling

After 3 days of culture, constructs were fixed and permeabilized according to the aforementioned procedure. For saturation of non-specific binding sites, samples were incubated in a saturation buffer composed of 1% (w/v) bovine serum albumin (BSA, Sigma A3311, France) and 0.05% (v/v) Tween-20 (Sigma P1379, France) in PBS for 1 hour at room temperature. Specific primary antibodies dilution (***Supplementary information 2***) were applied in saturation buffer overnight at 4°C. Then, secondary antibodies (***Supplementary information 2***) were diluted and applied for 1 hour at room temperature. The constructs were counterstained with DAPI at a concentration of 300 nM in PBS for 10 minutes at room temperature and investigated by confocal imaging. For negative controls, primary antibodies were excluded. Images were taken at the Centre Technologique des microstructures (University of Lyon, France) on a Zeiss LSM800 confocal microscope.

Transmission Electron Microscopy (TEM) Imaging

Bioprinted constructs were washed twice with phosphate buffer (PB, 0.1M) and subsequently incubated with 2.5% (v/v) glutaraldehyde (Sigma G5882, France) in PB for 2 hours at room temperature and finally washed again 3 times with PB solution. After dehydration, the samples were infiltrated, embedded in epoxy resin and polymerized for 3 days at 56 °C. Ultrathin sections (70-80 nm) were collected on Formvar-coated slot copper grids (Electron Microscopy Sciences), counterstained with 7% uranyl acetate in methanol solution and then in Reynolds' lead citrate. Images were taken at the Centre Technologique des Microstructures (University of Lyon, France) on a TEM Philips CM120 at 80 kV using a CCD camera GATAN Orius 200.

hVEGF ELISA quantification

hVEGF was quantified in culture supernatants of bioprinted constructs after 3 days of culture using a specific hVEGF ELISA Kit (Invitrogen KHG0111, France), according to manufacturer's protocol. Briefly, 100 µl of each supernatant were deposited on anti-human VEGF coated 96-well plates and stand for binding for 2 hours at room temperature. Unbound biological components were washed out using manufacturer's washing buffer. 100 µl of anti-hVEGF biotin-conjugated solution were then deposited into each well and incubated for 1 hour at room temperature before being washed 4 times with washing buffer to remove unbound biotin-conjugated anti-hVEGF antibody. 100 µl of streptavidin-HRP were then added to each well and incubated for 30 minutes at room temperature. During this step, streptavidin-HRP binds to the anti-hVEGF biotin-conjugated antibody. Finally, 100 µl of stabilized chromogen were added to each well and incubated for 30 minutes at room temperature. The enzymatic reaction was terminated by the

addition of 100 µL of manufacturer's stop solution and the absorbance of each well measured at 450 nm.

RESULTS

Mimicking Bruch's Membrane/RPE Complex

To simulate Bruch's Membrane, a 5-20 µm thick GelMa layer was coated on the surface of circular glass coverslips before seeding with RPE cells. Since we applied GelMa with high degree of substitution (80%), we did not experience the toxicity problem caused by unreacted methacrylic anhydride and oligo methacrylic acid byproducts (Yue *et al.*, 2015; Rose *et al.*, 2014).

Figure 1-A compares viability of RPE cells cultured on GelMa layer and on classical tissue culture plates (TCPs). As can be seen, RPE cells were viable and proliferate on GelMa layer over the studied one-week culture time.

Moreover, cell population significantly increased when culture was performed on GelMa coating ($p \leq 0.05$), proof of the positive impact of generating a Brunch-like membrane from GelMa for RPE layer sheet development. As a next step, RPE cells were labeled with PKH67 in order to directly monitor cells after inkjet bioprinting. The effect of this long lasting cell staining upon growth was first evaluated. **Figure 1-B** presents the growth comparison results between labelled PKH67 and non-labelled RPE cells. As a matter of fact, a negative effect of the labelling was observed in the early stages (day 1) of the RPE sheet development which was completely recovered after 3 days of culture ($p \leq 0.05$).

In second set of experiments, inkjet bioprinting effect upon the RPE sheet development on GelMa membrane was evaluated. To do so, freshly dissociated RPE were bioprinted on Brunch-like membrane and the behavior and growth of the cell population monitored. **Figure 1-C** depicts the

actual 80 µm nozzle very end filled with suspended RPE during inkjet bioprinting. The size of the suspended cells (15-20 µm) appears compatible with the nozzle size but with a clear limitation in term of number of cells being able to flow concomitantly through the nozzle aperture without clogging or strong loss of viability due to the presence of high shear stress.

Cell growth was then evaluated on both bioprinted and classically seeded RPE (5.10^4 cells per cm^2). As can be seen in **Figure 1-D**, a significant discrepancy in the metabolic activity rate of the bioprinted RPE was observed when compared to classically seeded cells. Thus, after 7 days of culture, the bioprinted RPE sheet which had shown a faster development in the 1-3 days period, evidenced a 25% lower metabolic activity.

Finally, **Figures 1-E** and **-F** present the surface of bioprinted RPE on GelMa Bruch-like membrane after 7 days on culture. Cells were distributed homogeneously within the printed area. Microphthalmia-associated transcription factor (MITF) and tight junction-associated protein (ZO1) labelling were performed in order to evaluate the functional maturation of the bioprinted RPE sheets. As can be seen, ZO1 was observed all over the obtained cell sheet, proof of the maturation of the sheet into a dense epithelial monolayer (Li and Poznansky, 1990). Moreover, the presence of MITF marker was also evidenced all over the sheet, proof of a fully functional and stable RPE layer.

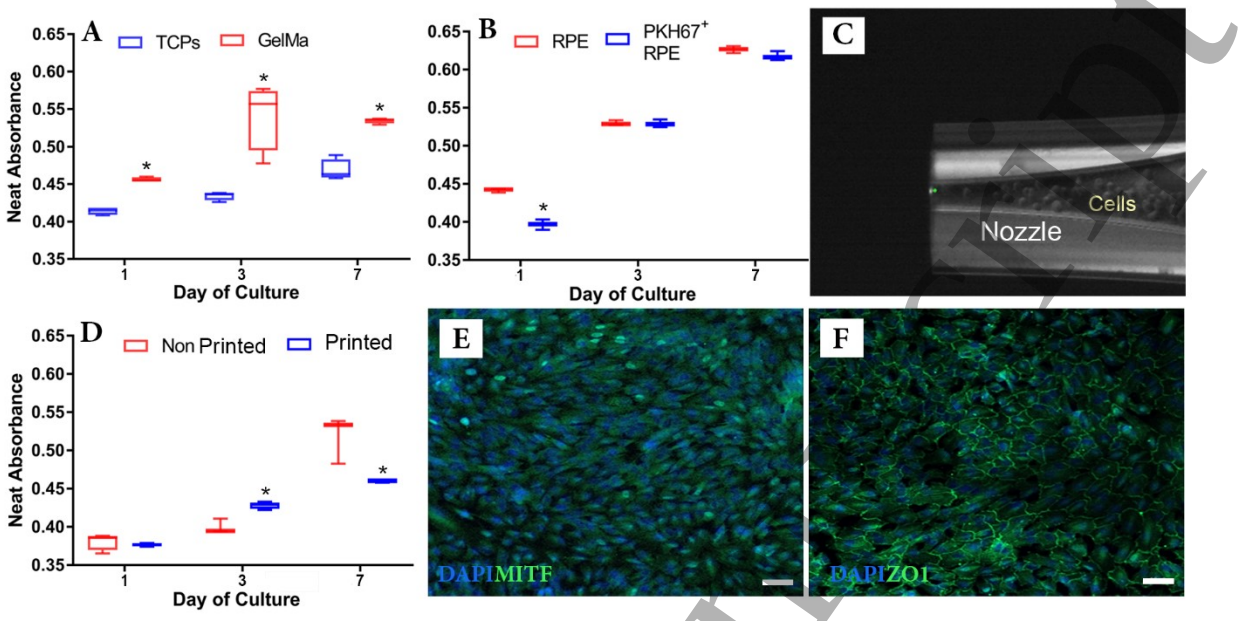

Figure 1. A) RPE population growth on GelMa coated layer and Tissue Culture plates (TCPs). B) RPE population growth of PKH67 labeled and non-labeled RPE cells. C) Close-up image of the bioprinted nozzle filled with RPE cells. D) Growth of bioprinted and seeded RPE cells on GelMa. E) MITF labelling (green, counter staining with DAPI in blue) showing the presence of Microphthalmia-associated Transcription Factor all over the RPE bioprinted sheet on GelMa brunch-like membrane. F) ZO1 labelling (green, counter staining with DAPI in blue) showing the distribution of tight junctions all over the RPE bioprinted sheet on GelMa brunch-like membrane. *Asterisks represent significant difference between groups in each day at p≤0.05. Scale bars: 50 µm (E&F).*

Isolation of enriched rod and cone photoreceptors

In order to be able to produce full retina tissues through inkjet bioprinting, photoreceptors shall be deposited at the surface of the bioprinted RPE sheet. These photoreceptor cells (PRs) were isolated from pig eyes according to the protocol depicted in **Figure 2-A**. Following isolation, enriched

population of rod and cone photoreceptors were observed by phase contrast imaging and identified through immunochemical labelling using retinal cell-type–specific antibodies (**Figure 2-B**). Phase contrast images clearly indicate a mixed population of dense cells with various shapes such as round or elongated forms, typical of rod and cone retinal cells. Nevertheless, it was clear from these images that the obtained isolated cells population was richer in rods than in cones. Rhodopsin-based labelling of rod cells (**Figure 2-C**) and opsin-based labelling of cone cells (**Figure 2-D** and **2-E**) also confirmed this observation. A purity of 95% was estimated for photoreceptors in the isolated population (Traverso *et al.*, 2003).

Another observation was that the obtained cell suspension was composed of single isolated cells, without any identified multicellular large size aggregates which might have been incompatible with the 80 µm diameter inkjet bioprinting nozzle.

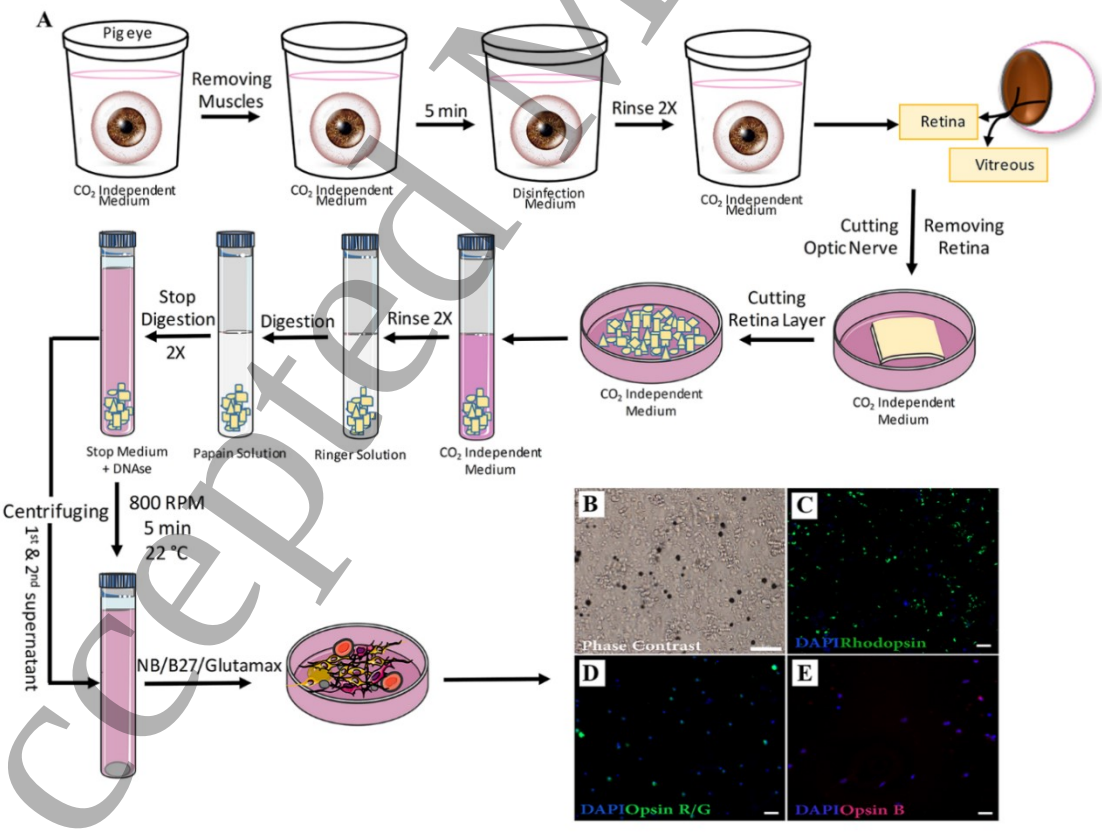

Figure 2. A) Schematic of photoreceptors isolation steps from pig eye. B) Phase contrast image of isolated photoreceptors. C) Fluorescence image of isolated photoreceptors labelled with anti-rhodopsin antibodies. C) Fluorescence image of isolated photoreceptors labelled with anti-opsin R/G antibodies. E) Fluorescence image of isolated photoreceptors labelled with anti-opsin B antibodies. Nuclei were counterstained with DAPI (blue). *Scale bars: 50 µm (B) and 20 µm (C-E).*

Mimicking Bruch's membrane/RPE/PRs complex through layer-by-layer cellular inkjet bioprinting

Bioprinted RPE cell sheets on GelMa Brunch-like membranes were then used to recapitulate photoreceptors/RPE complexes. To do so, freshly isolated photoreceptors were bioprinted onto 7-days matured RPE cell sheets. **Figure 3-A** depicts the distribution of the PRs on RPE cell sheet right after bioprinting. As can be seen, PRs were homogeneously distributed over the RPE cell sheet, proof of the capability of the inkjet bioprinting technique to spread mature and differentiated photoreceptors over a large surface (here up to 1 cm^2). This is where the use of bioprinting has the major impact: recapitulating PR sheet from rare, mature and freshly isolate cell. For sake of comparison, PRs were also bioprinted on bare TCP surface. In that case, the bioprinted drops did not spread on the surface of the underneath RPE layer, leading to non-homogeneous distribution of the photoreceptors (data not show).

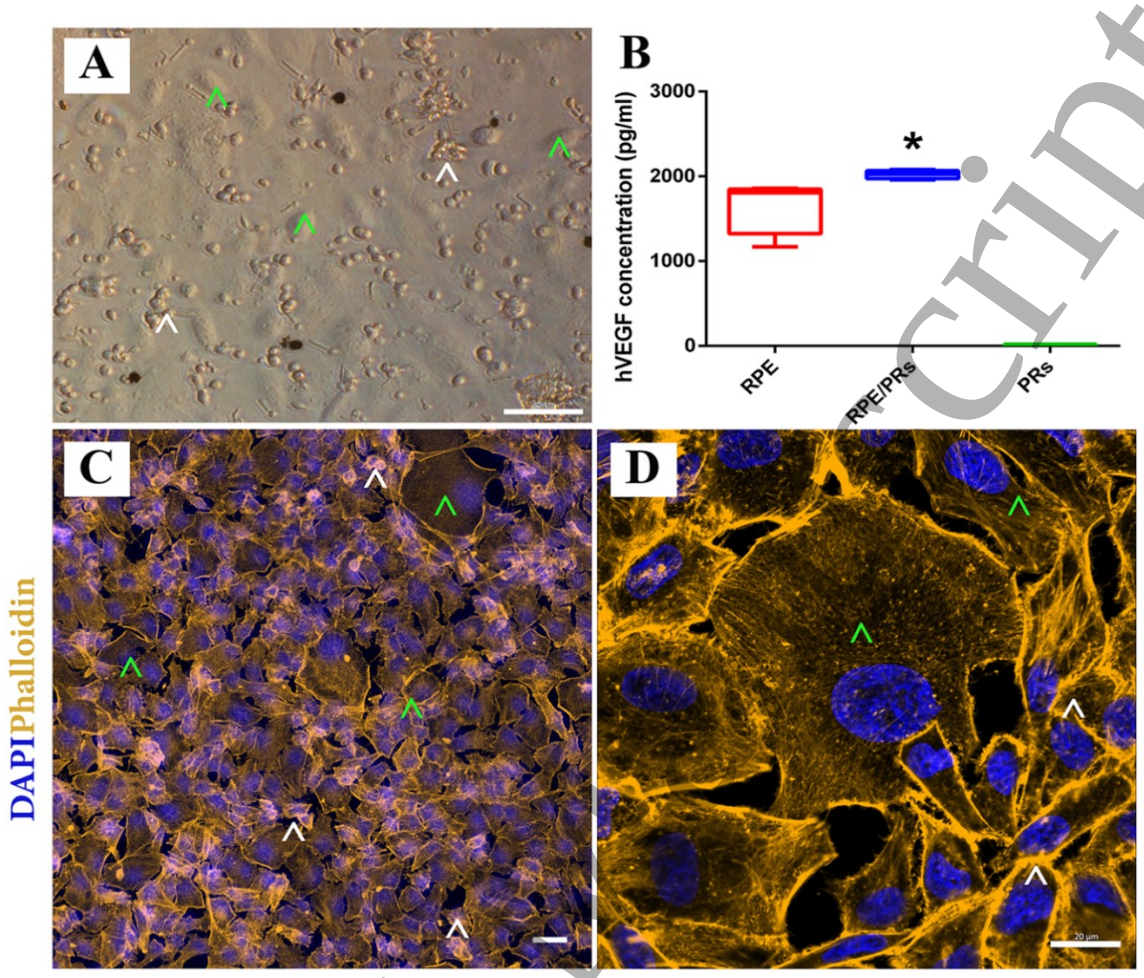

Figure 3. A) Phase contrast image of bioprinted PRs on RPE layer. B) Quantitative detection of released hVEGF from constructs, 3 days after bioprinting. C and D) Fluorescence microscopy images of cellular actin filaments (yellow) on GelMa/RPE/PRs constructs. Nuclei are counterstained with DAPI (blue). Green and white arrows show RPE and PR cells, respectively. *Asterisk represents significant difference at $p \leq 0.05$. Scale bars: 50 µm (A & C) and 20 µm (D).*

hVEGF was originally recognized as an endothelial angiogenic and vasopermeability factor secreted in retina by RPE cells. In order to validate that the RPE layer and the RPE/PR constructs we had produced through bioprinting were still producing this important factor, hVEGF was

quantified in the culture supernatants. **Figure 3-B** presents the results of this quantification in which ng/mL levels of hVEGF were found in the RPE and RPE/PR constructs. As a control, hVEGF production from PR was shown to be negligible.

Then, the distribution and the organization of the actin filaments within the RPE/PR constructs were evaluated through phalloidin staining and laser confocal microscopy, 3 days after PR bioprinting. As can be seen in **Figure 3-C** and **3-D**, a dense network of actin filaments was evidenced with a clear identification of large and spread RPE cells (green asterisk) together with small and compact PR cells (white arrows). Interaction and topology between the two cell layers, i.e. RPE and PR, were not reachable using the present technique and a complementary study using confocal microscopy and cell phenotype specific labelling was implemented.

ZO1, MITF, Rhodopsin, Opsin red/green, Opsin blue and PNA were then used as specific markers for immunohistological analysis. **Figure 4** depicts the confocal microscopy images obtained. A first observation can be made about the organization of the RPE/PR constructs which appear to be orientated in separated layers. Indeed, as can be seen in **Figure 4-A**, a clear layered organization was found between the ZO1 labelled tight junction of the RPE layer and part of the DAPI labelled nuclei. This observation proves then that the ZO1 labelled cells (and their nuclei) were localized in the lowest part of the construct, while unlabeled cells (PRs) can be found on the upper layer of the construct. The same conclusion was obtained from MITF labelled constructs (**Figure 4-B**).

Then, to ensure that PRs bioprinted on top of RPE sheet retain their initial differentiation markers, 3D bioprinted constructs were stained with different PR specific markers: Rhodopsin, Opsin blue, Opsin red/green, and PNA. As can be seen, all these markers were identified in the obtained construct (**Figure 4-C, -D, -E and –F**). Interestingly, these markers were found in the lower part of the construct, suggesting that PR tails were partially inserted within the RPE layer.

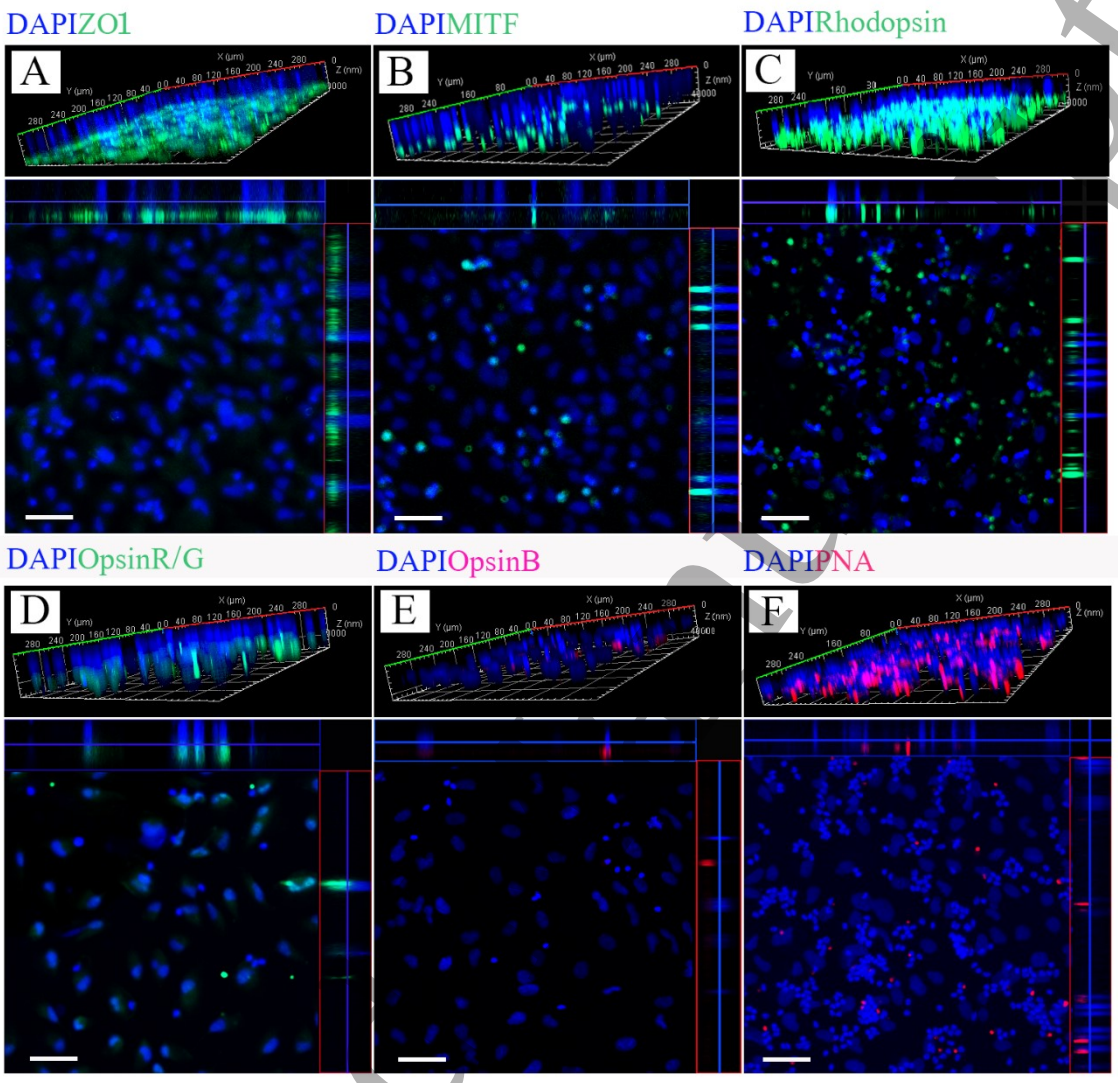

Figure 4. Confocal fluorescence microscopy images of bioprinted constructs. A: ZO1 immunolabelling. B: MITF immunolabelling. C: Rhodopsin immunolabelling. D: Opsin R/G immunolabelling. E: Ospin B immunolabelling. F: PNA immunolabelling. Nuclei are counterstained with DAPI (blue). The top images show 3D view and bottom images show ortho view of the constructs. *Scale bars: 50 µm (A-F).*

Electron Microscopy and Photoreceptor Outer Segment (POS) Phagocytosis by RPE cells after bioprinting

Electron microscopy of RPE cells cultured on GelMa coated substrates revealed a polarized RPE sheet with many features of RPE morphology, including numerous dense bodies in the cytoplasm, and apical electron-dense structures (**Figure 5-A**). Basolateral infolds (Bi) in RPE cells adjacent to the GelMa membrane and adherent Junctions (Aj) in apical borders of RPE cells were also clearly visible (**Figure 5-C**). Not bioprinted control PRs, depicted in **Figure 5-B,** also showed the expected shapes of outer segments with high electron density.

We assessed further the RPE-PRs interactions upon bioprinting at ultrastructural level. After 24h cultivation of complete bioprinted GelMa/RPE/PRs constructs, internal structure of the phagocytized POS can be observed (**Figures 5-D to -F**). Numerous microvilli (Mv) were also observed on the apical RPE of the bioprinted final construct (**Figure 5-F**).

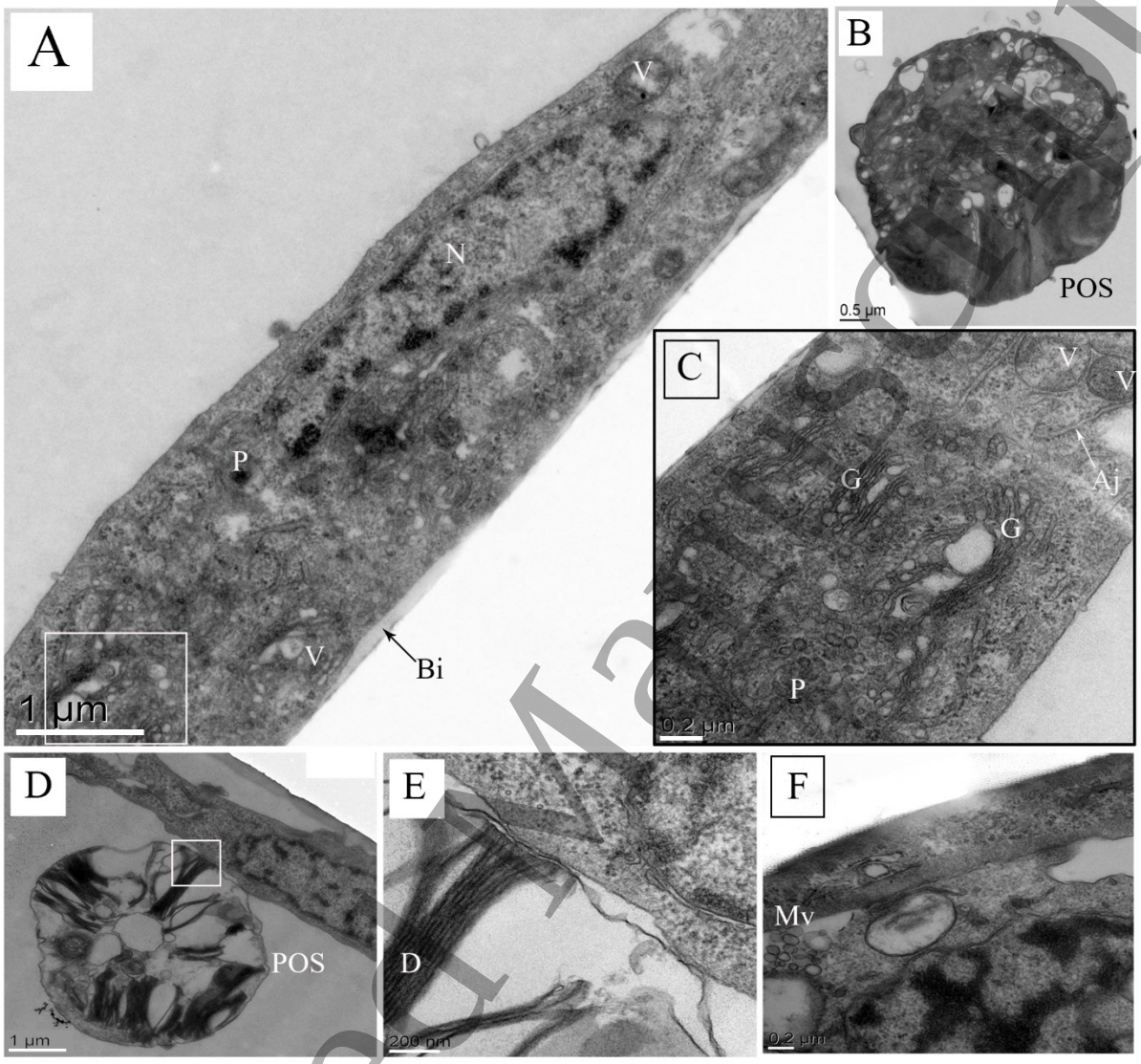

Figure 5. Electron micrographs depicting ultrastructures of 3D bioprinted constructs. A & C) RPE sheet, B) photoreceptor outer segment (POS) of isolated PRs, D-F) POS phagocytosis by RPE sheet 24h after cultivation of complete bioprinted construct.

V: vesicular compartments; N: nuclei; P: pigment molecules; Bi: basolateral infolds; G: Golgi; Aj: adherent junctions; D: photoreceptor disks; Mv: microvilli. *Scale bars: 1 µm (A & D), 0.5 µm (B), 0.2 µm (C, E & F).*

DISCUSSION

The retina is a complex neuro-sensory tissue responsible for primary visual signal processing. In some ocular pathologies such as age-related macular degeneration and retinitis pigmentosa, degeneration or atrophy of RPE cells in retina layer, directly followed by a loss of the associated photoreceptor cells, lead to vision deterioration. Most of native RPE functions such as gene expression profile, ability of cells to form tight junctions, polarized cytokine secretion, and ability to phagocytose POS are related to 3D structure of retina (Miyagishima *et al.*, 2017; Hsiung *et al.*, 2015). This is the main reason why multiple ongoing efforts for regeneration of damaged retina have been focused on preservation of 3D layered structure of retinal cells and their secreted matrix.

In the present study, we applied 3D inkjet bioprinting technique as a novel carrier-free method to simulate retina tissue with 3D multi-layered structure, without any carrier material. In a first step, a Bruch's membrane model was designed from GelMa thin layer, in order to achieve a biomimetic physiological microenvironment of the native retina. This part is of upmost importance since this is where the RPE layer is separated by a membrane from the underlying fenestrated choroidal capillaries of the eye. As GelMa is a gelatin derivative material, it contains significant amounts of matrix metalloproteinase peptide motifs, which positively affect cellular function (Yue *et al.*, 2015). Therefore, this design was found to suit well the development of RPE cells, as observed in our results (**Figure 1-A**). After mimicking Bruch's membrane, a piezoelectric inkjet printer was used to develop a retina cell bioprinting process taking advantage of the high resolution of the machine X/Y axis (5 µm) and the extremely low deposition volume (down to 180 pL).

In our carrier-free bioprinting approach, cell suspension was directly deposited during bioprinting process and probably due to the absence of any other biomaterial, no clogging occurred within the

capillary nozzle (**Figure 1-C**). Compared to extrusion method, inkjet bioprinting commonly requires low viscosities to avoid nozzle clogging and control potential for jamming. Low viscosity bioinks is also desirable to control fluid shear stress, known as a crucial factor that unfavorably affects viability, signaling and protein expression after bioprinting (Chimene *et al.*, 2016; Ozbolat, 2015). One possible reason is that, excessive stress probably dispatches cells by disrupting cellular membrane (Blaeser *et al.*, 2016).

During bioprinting with hydrogel cell laden bioinks, when high viscosity materials travel through the extrusion nozzle, cells are expose to high levels of shear stress which affect their immediate viability and ultimately their functionalities. Our hypothesis is that, short-time (100 µs) exposure to low levels of shear stress (Calculated using the nozzle geometry and a viscosity of $1.00E^{-03}$ Pa.s: Wall Shear rate: $1.31E^{+08}$ s^{-1}; Wall Shear stress: $1.31E^{+05}$ Pa (FlowTips® Program, 3d.FAB, France) in our carrier-free system does not affect cell viability immediately after printing (day 1), but might still induce long-term alterations in the proliferation potential of cells that survived the printing process (day 7) (**Figure 1-D**). However, although bioprinting process has reduced RPE proliferation rate over a week, the bioprinted cells adapted with process condition, survived and continued their proliferation after printing.

Without ink materials, we were also capable of bioprinting cell densities closer to the figures of a native tissue (Ozbolat, 2015). Indeed, during inkjet bioprinting, single drop ejected from the nozzle has, under our experimental conditions, a volume of 300 pL. 52 drops were dispensed per deposition location leading to an estimated cell density of around 93 ± 15 RPE cells per deposition. This will be of high importance when the technique will be applied to the deposition of highly differentiated non-proliferative cells such as photoreceptors.

Furthermore, our approach as well helps RPE cells to stack together for formation of monolayer sheet. Indeed, carrier-free deposition may also facilitate cellular maturation after bioprinting and GelMa coating probably guides cells to form monolayer sheet faster. In RPE sheets, extracellular matrix and secreted adhesion molecules are crucial regulators of cell behavior, which prevent cell apoptosis and allow an easy manipulation during subsequent transplantation. In fact, intracellular tight junction formation in RPE monolayer plays an important role in carrying out retina functions (Kamao *et al.*, 2014). Accordingly, we demonstrated that, bioprinted RPE cells positively express typical membrane-associated proteins such as ZO1 and MITF, similar to that of native RPE sheet *in vivo* (**Figures 1-E and –F**). These factors were identified in 3D bioprinted constructs, after Z-stack 3D confocal imaging (**Figures 4-A & -B**). ZO1 is a common adaptor protein associated with tight junctions, anchoring junctional macromolecular complexes to cytoplasmic actin (Obert *et al.*, 2017; Liao *et al.*, 2010). MITF is also considered as essential for terminal pigment differentiation in the RPE (Westenskow *et al.*, 2009). These proteins are polarized and actively interact with other membrane proteins/receptors, cell adhesion molecules, and the cytoskeleton to regulate epithelial cell morphology and assemble signaling cascades.

In the next step, we had isolated PRs using a well-defined protocol with the purpose of applying them as the second cellular layer of bioprinted retina (**Figure 2-A**). PRs (rods and cones) are highly specialized neurons with stacks of photosensitive disks that have special morphology and express different rod- or cone-specific markers. Although, we have no direct evidence on proportion of isolated rod cells to cones, based on Traverso ‘s protocol, isolated cells probably have rod-cone ratio between 1.3 and 2 (Traverso *et al.*, 2003). In a classic approach, we then characterized isolated cells through imaging, morphological analysis and immunofluorescent labeling of light-sensitive receptor proteins such as rhodopsin, opsin R/G and opsin B (**Figures 2-B to –E**).

Afterward, primary isolated PRs were bioprinted on RPE/GelMa layer to form 3D retina constructs. For RPE cells, we designed printing pattern based on our study plan. Since we needed a RPE monolayer sheet, and for cells maturation we should incubate them for at least a week, we decided to make a gap between RPE depositions, so that the cells had enough space for growth and maturation (***Supplementary Information 1***). Over the studied one-week culture time, we had virtually no non-RPE regions. We next showed full epithelium structure of cells by immunostaining images of ZO1 marker as well as hVEGF measurement.

In contrast, for obtaining a PR surface coverage close to the native one, and since photoreceptor cell body size is less than that of RPE cell, we had increased and optimized the number of deposition location through a trial and error bioprinting of PRs on RPE/GelMa layer.

Once PR bioprinting feasibility was proven, we confirmed the presence of positioned PRs, 3 days after bioprinting with phase-contrast imaging and cytoskeleton staining **(Figures 3-A, –C and –D)**. Although without specific staining it is difficult to distinguish PRs from underlying RPE cells, expected morphology of PRs with long outer segments are evident in **Figure 3-A**.

As another part of our study, we investigated the possibility that human RPE cells secrete angiogenic factors such as hVEGF after bioprinting process **(Figure 3-B)**. hVEGF protein is a potent endothelial factor which promotes angiogenesis and its optimal levels is essential for maintaining choriocapillaris and choroidal vessels *in vivo* (Adamis *et al.*, 1993).

Obviously, hVEGF must be secreted within a defined concentration range to be biologically functional. Blaauwgeers *et al.* have reported that primary RPE cells secrete between 0.2 ng/ml on their apical side to 11 ng/ml on their basal side (Blaauwgeers *et al.*, 1999). There numbers correlated well with our results since the concentration of hVEGF found in the construct culture medium in our experimental conditions was 2 ± 0.06 ng/ml.

ARPE19 cells retained their growth-adapted phenotype when cultured under standard conditions, indicated by expended cell morphology and interdigitated cell-cell junctions. The exact constituents of the proteins released from RPE cells are available in the literatures. For example, McLenachan *et al*. reported that, decellularized ARPE19-ECM displayed immunoreactivity for proteins found in the inner layers of Bruch's membrane, including fibronectin, vitronectin, collagens IV, and V as well as laminin-α5 (McLenachan et al., 2017). Here, we hypothesized that this effective production of secreted hVEGF from bioprinted RPE cells may be due to known roles of 3D structure of ECM. Indeed, with bioprinting, we had organized RPE cells in a layered way on top of a GeMa Bruch's like membrane which can provide mechanical support for next angiogenesis. In other words, GelMa can, *in vitro,* induce recapitulation of the native RPE microenvironment and provided enriched ECM conditions for RPE cell culture.

Such a role for 3D matrix has been previously confirmed by others (Mousa *et al.*, 1999; Farjood and Vargis, 2018) and is based on the observation that ECM of RPE cells can cause increased secretion of angiogenic growth factors. Despite, certain importance of hVEGF for stimulating vascular permeability, RPE-secreted hVEGF has also neuroprotective effects for neural retina and are anti-apoptotic agent for retinal neurons (Nishijima *et al.*, 2007; Kilic *et al.*, 2006).

A step forward in the present study has been the immunofluorescent detection of specific molecular markers within our retina constructs. Thus, we were able to detect considerable expression levels of ZO1 and MITF as membrane-associated proteins of RPE layer but also rhodopsin, opsin R/G and opsin B as light-sensitive proteins expressed in rod and cone outer segments, and PNA as cone ECM marker after bioprinting (**Figure 4**). One of the main results here is the fact that some nuclei are co-localized with RPE markers and some co-localized with PR markers. Also, some nuclei are in the lower part of the construct and other in the upper part.

Therefore, part of immunostaining results are difficult to analyze. However, these data indicate that bioprinting process reliably and robustly produces a GelMa/RPE/PRs complex with adequate functionality comparable with that of native retina. As cultivation and maintenance of primary isolated PRs for long-term periods is a key challenge for *in vitro* studies, we just experimented above behaviors 3 days after incubation. It was well known that, after dissociation from retinal environment, isolated PRs lose their functional integrity in the primary cell culture (Reidel *et al.*, 2006; Fintz *et al.*, 2003).

Different studies on retinal cells recommend that retinal PRs require specific trophic factors or feeder layers for long-term culture (Fintz *et al.*, 2003). Interactions between PRs and neighboring Müller glial cells is also of important for PRs function and survival (Vecino *et al.*, 2016). Therefore, long-term incubation of bioprinted constructs in the native environment of PRs should be done in future to investigate potential value of bioprinting for studying sight-threatening diseases.

The present observation of the immunofluorescent labelled constructs through confocal microscopy is one of the first attempt in assessing biological characterization of bioprinted retina construct. Indeed, even if in one of the few available articles about retina bioprinting, Shi et al. reported excellent viability of both ARPE-19 and Y79 cell lines after bioprinting (Shi *et al.*, 2017), no biological assessment related to the specific functionality of bioprinted cells was performed. Here, we have shown for the first time that both bioprinted RPE and PRs expressed essential transcription factors. This observation is crucial for the validation of functional GelMa/RPE/PRs bioprinted constructs for future clinical applications.

To further expand our findings about functionality of bioprinted constructs, we assessed cells' microstructure through electron microscopy (**Figure 5**) and showed specific phagocytosis of POS

by apical surface of RPE cells. Just like in the case of the biological characterization of bioprinted retinal cells, previous studies have not addressed the phagocytosis of POS after bioprinting. RPE cells phagocyte POS fragments to remove the photo-oxidative residual bodies that accumulate daily during phototransduction process (Penberthy *et al.*, 2018). Many studies have confirmed that any dysfunction in POS phagocytosis pathway may lead to different retinal pathologies and eventual blindness (Carr *et al.*, 2009; Nandrot *et al.*, 2004; Mao and Finnemann, 2012; Penberthy *et al.*, 2018). For example, deficiency or mutation of phagocytosis associated molecular factors such as MerTK and PtdSer receptors may cause rapid RPE degradation and retinitis pigmentosa pathology (Burstyn-Cohen *et al.*, 2012; Ostergaard *et al.*, 2011; Penberthy *et al.*, 2018). Expected morphology of RPE cells in TEM images and development of epithelial monolayer, which previously was established by ZO1 and MITF protein expressions, are of great importance in phagocytic capacity of RPE cells after bioprinting. This topic has been mentioned in literatures, when relationship between POS phagocytosis pathway and RPE differentiation has been studied (Mao and Finnemann, 2012; Mazzoni *et al.*, 2014). With further evaluation of the ultrastructure images of 3D bioprinted constructs, adjacency of POS disk fragments with apical microvilli of RPE layer were observed (**Figures 5-D to –F**). Presence of RPE microvilli is essential for functional *in vivo* phagocytosis and is a main challenge during *in vitro* simulation of this phenomenon (Feng *et al.*, 2002). Here we can claim that, using bioprinting approach, we succeeded in binding PRs' outer segment to RPE apical microvilli, recapitulating finely an *in vivo* phenomenon where direct contact of outer segments with RPE microvilli contributes to phagocytosis.

In summary, we successfully engineered part of the complex 3D structure of the retina using inkjet bioprinting technology in a carrier-free approach. Layer-by-layer printing of photoreceptor cells

on RPE monolayer did not alter cells' biological functions such as morphology, viability and expression of specific proteins, leading to an engineered construct with considerable resemblance to native retina. While no direct tests were conducted to assay outer segment phagocytosis and visual cycle activity, the protein expression data and microstructure imaging suggested that after bioprinting, both RPE and PRs were capable of performing specific retinal functions. These functional studies of the obtained constructs will be have to be examined in depth in the future.

AUTHOR INFORMATION

Corresponding Authors

*E-mails: Elahe Masaeli (elahe.masaeli@royaninstitute.org) or Christophe Marquette (christophe.marquette@univ-lyon1.fr)

Author Contributions

Conceived and designed the experiments: EM VF FK MHN-E CM. Performed the experiments: EM CM. Analyzed the data: EM CM FK. Wrote the paper: EM CM SP.

ACKNOWLEDGMENT

Confocal and Transmission Electron Microscopy experiments were performed at the Centre Technologique des Microstructures (University of Lyon, France) under the supervision of Christelle Fabrer-Boulé and Veronica La Padula.

FUNDING SOURCES

This research did not receive any specific grant from funding agencies in the public, commercial, or not-for-profit sectors.

REFERENCES

Adamis A, Shima D, Yeo K-T, Yeo T, Brown L, Berse B, Damore P and Folkman J 1993 Synthesis and secretion of vascular permeability factor/vascular endothelial growth factor by human retinal pigment epithelial cells *Biochem Biophys Res Commun* **193** 631-8

Blaauwgeers H G, Holtkamp G M, Rutten H, Witmer A N, Koolwijk P, Partanen T A, Alitalo K, Kroon M E, Kijlstra A and van Hinsbergh V W 1999 Polarized vascular endothelial growth factor secretion by human retinal pigment epithelium and localization of vascular endothelial growth factor receptors on the inner choriocapillaris: evidence for a trophic paracrine relation *The American journal of pathology* **155** 421-8

Blaeser A, Duarte Campos D F, Puster U, Richtering W, Stevens M M and Fischer H 2016 Controlling shear stress in 3D bioprinting is a key factor to balance printing resolution and stem cell integrity *Advanced healthcare materials* **5** 326-33

Burstyn-Cohen T, Lew E D, Través P G, Burrola P G, Hash J C and Lemke G 2012 Genetic dissection of TAM receptor-ligand interaction in retinal pigment epithelial cell phagocytosis *Neuron* **76** 1123-32

Carr A-J, Vugler A, Lawrence J, Chen L L, Ahmado A, Chen F K, Semo M a, Gias C, da Cruz L and Moore H D 2009 Molecular characterization and functional analysis of phagocytosis by human embryonic stem cell-derived RPE cells using a novel human retinal assay *Mol Vis* **15** 283

Chimene D, Lennox K K, Kaunas R R and Gaharwar A K 2016 Advanced bioinks for 3D printing: a materials science perspective *Ann Biomed Eng* **44** 2090-102

da Silva G R, Junior A D C, Saliba J B, Berdugo M, Goldenberg B T, Naud M C, Ayres E, Orefice R L and Cohen F B 2011 Polyurethanes as supports for human retinal pigment epithelium cell growth *Int J Artif Organs* **34** 198-209

De Maria C, Vozzi G and Moroni L 2017 Multimaterial, heterogeneous, and multicellular three-dimensional bioprinting *Mrs Bull* **42** 578-84

Dias A, Kingsley D and Corr D 2014 Recent Advances in Bioprinting and Applications for Biosensing *Biosensors* **4** 111

Farjood F and Vargis E 2018 Novel devices for studying acute and chronic mechanical stress in retinal pigment epithelial cells *Lab Chip* **18** 3413-24

Feng W, Yasumura D, Matthes M T, LaVail M M and Vollrath D 2002 Mertk triggers uptake of photoreceptor outer segments during phagocytosis by cultured retinal pigment epithelial cells *J Biol Chem* **277** 17016-22

Fintz A-C, Audo I, Hicks D, Mohand-Said S, Léveillard T and Sahel J 2003 Partial characterization of retina-derived cone neuroprotection in two culture models of photoreceptor degeneration *Investigative ophthalmology & visual science* **44** 818-25

Guillotin B and Guillemot F 2011 Cell patterning technologies for organotypic tissue fabrication *Trends Biotechnol* **29** 183-90

Hsiung J, Zhu D and Hinton D R 2015 Polarized Human Embryonic Stem Cell-Derived Retinal Pigment Epithelial Cell Monolayers Have Higher Resistance to Oxidative Stress-Induced Cell Death Than Nonpolarized Cultures *Stem cells translational medicine* **4** 10-20

Jorge I R-D, Bimeng Z, Daniel R, Zhi-dong S and Tao X 2012 High throughput miniature drug-screening platform using bioprinting technology *Biofabrication* **4** 035001

Kamao H, Mandai M, Okamoto S, Sakai N, Suga A, Sugita S, Kiryu J and Takahashi M 2014 Characterization of human induced pluripotent stem cell-derived retinal pigment epithelium cell sheets aiming for clinical application *Stem cell reports* **2** 205-18

Kilic Ü, Kilic E, Järve A, Guo Z, Spudich A, Bieber K, Barzena U, Bassetti C L, Marti H H and Hermann D M 2006 Human vascular endothelial growth factor protects axotomized retinal ganglion cells in vivo by activating ERK-1/2 and Akt pathways *J Neurosci* **26** 12439-46

Kolesky D B, Truby R L, Gladman A S, Busbee T A, Homan K A and Lewis J A 2014 3D bioprinting of vascularized, heterogeneous cell-laden tissue constructs *Advanced materials* **26** 3124-30

Li C and Poznansky M J 1990 Characterization of the ZO-1 protein in endothelial and other cell lines *J Cell Sci* **97** 231-7

Liao J-L, Yu J, Huang K, Hu J, Diemer T, Ma Z, Dvash T, Yang X-J, Travis G H and Williams D S 2010 Molecular signature of primary retinal pigment epithelium and stem-cell-derived RPE cells *Hum Mol Genet* **19** 4229-38

Luo X, Heidinger V r, Picaud S, Lambrou G, Dreyfus H, Sahel J and Hicks D 2001 Selective excitotoxic degeneration of adult pig retinal ganglion cells in vitro *Investigative ophthalmology & visual science* **42** 1096-106

Mao Y and Finnemann S C 2012 *Retinal Degeneration*: Springer) pp 285-95

Mazzoni F, Safa H and Finnemann S C 2014 Understanding photoreceptor outer segment phagocytosis: use and utility of RPE cells in culture *Exp Eye Res* **126** 51-60

McLenachan S, Hao E, Zhang D, Zhang L, Edel M and Chen F 2017 Bioengineered Bruch's-like extracellular matrix promotes retinal pigment epithelial differentiation *Biochemistry and biophysics reports* **10** 178-85

Miyagishima K J, Wan Q, Miller S S and Bharti K 2017 A basis for comparison: sensitive authentication of stem cell derived RPE using physiological responses of intact RPE monolayers *Stem cell and translational investigation* **4**

Mokhtarinia K, Nourbakhsh M S, Masaeli E, Entezam M, Karamali F and Nasr-Esfahani M H 2018 Switchable phase transition behavior of thermoresponsive substrates for cell sheet engineering *Journal of Polymer Science Part B: Polymer Physics*

Mousa S A, Lorelli W and Campochiaro P A 1999 Role of hypoxia and extracellular matrix-integrin binding in the modulation of angiogenic growth factors secretion by retinal pigmented epithelial cells *J Cell Biochem* **74** 135-43

Nandrot E F, Kim Y, Brodie S E, Huang X, Sheppard D and Finnemann S C 2004 Loss of synchronized retinal phagocytosis and age-related blindness in mice lacking αvβ5 integrin *J Exp Med* **200** 1539-45

Nishijima K, Ng Y-S, Zhong L, Bradley J, Schubert W, Jo N, Akita J, Samuelsson S J, Robinson G S and Adamis A P 2007 Vascular endothelial growth factor-A is a survival factor for retinal neurons and a critical neuroprotectant during the adaptive response to ischemic injury *The American journal of pathology* **171** 53-67

Obert E, Strauss R, Brandon C, Grek C, Ghatnekar G, Gourdie R and Rohrer B 2017 Targeting the tight junction protein, zonula occludens-1, with the connexin43 mimetic peptide, αCT1, reduces VEGF-dependent RPE pathophysiology *Journal of Molecular Medicine* **95** 535-52

Ostergaard E, Duno M, Batbayli M, Vilhelmsen K and Rosenberg T 2011 A novel MERTK deletion is a common founder mutation in the Faroe Islands and is responsible for a high proportion of retinitis pigmentosa cases *Mol Vis* **17** 1485

Ozbolat I T 2015 Scaffold-based or scaffold-free bioprinting: competing or complementing approaches? *Journal of Nanotechnology in Engineering and Medicine* **6** 024701

Penberthy K K, Lysiak J J and Ravichandran K S 2018 Rethinking phagocytes: Clues from the retina and testes *Trends Cell Biol* **28** 317-27

Pourchet L J, Thepot A, Albouy M, Courtial E J, Boher A, Blum L J and Marquette C A 2017 Human Skin 3D Bioprinting Using Scaffold-Free Approach *Adv Healthc Mater* **6** 1601101

Ramsden C M, Powner M B, Carr A-J F, Smart M J, da Cruz L and Coffey P J 2013 Stem cells in retinal regeneration: past, present and future *Development* **140** 2576-85

Reidel B, Orisme W, Goldmann T, Smith W C and Wolfrum U 2006 Photoreceptor vitality in organotypic cultures of mature vertebrate retinas validated by light-dependent molecular movements *Vision research* **46** 4464-71

Rose J, Pacelli S, Haj A, Dua H, Hopkinson A, White L and Rose F 2014 Gelatin-based materials in ocular tissue engineering *Materials* **7** 3106-35

Shi P, Tan E Y S, Yeong W Y and Laude A 2017 Hybrid three-dimensional (3D) bioprinting of retina equivalent for ocular research

Shi P, Tan Y S E, Yeong W Y, Li H Y and Laude A 2018 A bilayer photoreceptor-retinal tissue model with gradient cell density design: A study of microvalve-based bioprinting *Journal of tissue engineering and regenerative medicine* **12** 1297-306

Singh R, Cuzzani O, Binette F, Sternberg H, West M D and Nasonkin I O 2018 Pluripotent Stem Cells for Retinal Tissue Engineering: Current Status and Future Prospects *Stem Cell Reviews and Reports* **14** 463-83

Tasoglu S and Demirci U 2013 Bioprinting for stem cell research *Trends Biotechnol* **31** 10-9

Tomita M, Lavik E, Klassen H, Zahir T, Langer R and Young M J 2005 Biodegradable polymer composite grafts promote the survival and differentiation of retinal progenitor cells *Stem Cells* **23** 1579-88

Traverso V r, Kinkl N, Grimm L, Sahel J and Hicks D 2003 Basic Fibroblast and Epidermal Growth Factors Stimulate Survival in Adult Porcine Photoreceptor Cell Cultures *Investigative Ophthalmology & Visual Science* **44** 4550-8

Trese M, Regatieri C V and Young M J 2012 Advances in Retinal Tissue Engineering *Materials* **5** 108

Tropepe V, Coles B L, Chiasson B J, Horsford D J, Elia A J, McInnes R R and van der Kooy D 2000 Retinal stem cells in the adult mammalian eye *Science* **287** 2032-6

Umemoto T, Yamato M, Nishida K and Okano T 2013 Regenerative medicine of cornea by cell sheet engineering using temperature-responsive culture surfaces *Chin Sci Bull* **58** 4349-56

Vecino E, Rodriguez F D, Ruzafa N, Pereiro X and Sharma S C 2016 Glia–neuron interactions in the mammalian retina *Progress in retinal and eye research* **51** 1-40

Westenskow P, Piccolo S and Fuhrmann S 2009 β-catenin controls differentiation of the retinal pigment epithelium in the mouse optic cup by regulating Mitf and Otx2 expression *Development* **136** 2505-10

Xu T, Zhao W, Zhu J M, Albanna M Z, Yoo J J and Atala A 2013 Complex heterogeneous tissue constructs containing multiple cell types prepared by inkjet printing technology *Biomaterials* **34** 130-9

Yaji N, Yamato M, Yang J, Okano T and Hori S 2009 Transplantation of tissue-engineered retinal pigment epithelial cell sheets in a rabbit model *Biomaterials* **30** 797-803

Yang J, Yamato M, Nishida K, Hayashida Y, Shimizu T, Kikuchi A, Tano Y and Okano T 2006 Corneal epithelial stem cell delivery using cell sheet engineering: not lost in transplantation *J Drug Target* **14** 471-82

Yao J, Tao S L and Young M J 2011 Synthetic Polymer Scaffolds for Stem Cell Transplantation in Retinal Tissue Engineering *Polymers* **3** 899

Yu Z, Rui Y, Liliang O, Hongxu D, Ting Z, Kaitai Z, Shujun C and Wei S 2014 Three-dimensional printing of Hela cells for cervical tumor model in vitro *Biofabrication* **6** 035001

Yue K, Trujillo-de Santiago G, Alvarez M M, Tamayol A, Annabi N and Khademhosseini A 2015 Synthesis, properties, and biomedical applications of gelatin methacryloyl (GelMA) hydrogels *Biomaterials* **73** 254-71

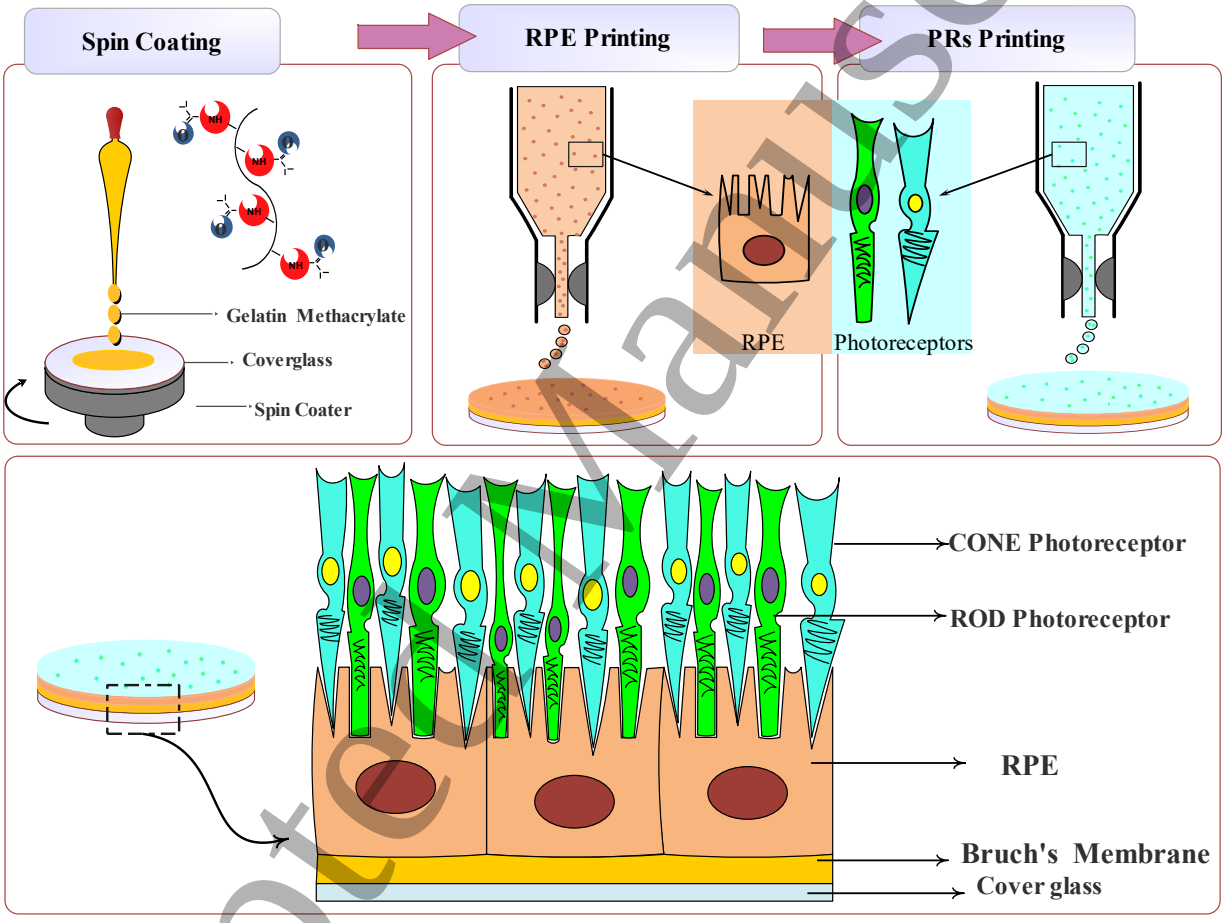

In this study, a unique inkjet-based bioprinter was applied to deposit matured and differentiated photoreceptors (PRs) on retina pigmented epithelium (RPE) layer in a predefined arrangement to create complex double-cell sheets.